Biogeosciences

Drivers of future seasonal cycle changes in oceanic pCO$_2$

M. Angeles Gallego[1], **Axel Timmermann**[2,3,4], **Tobias Friedrich**[2], and **Richard E. Zeebe**[1]

[1]Department of Oceanography, School of Ocean and Earth Sciences and Technology,
University of Hawaii at Manoa, Honolulu, Hawaii, USA
[2]International Pacific Research Center, School of Ocean and Earth Sciences and Technology,
University of Hawaii at Manoa, Honolulu, Hawaii, USA
[3]Center for Climate Physics, Institute for Basic Science (IBS), Busan, South Korea
[4]Pusan National University, Busan, South Korea

Correspondence: M. Angeles Gallego (mdla@hawaii.edu)

Abstract. Recent observation-based results show that the seasonal amplitude of surface ocean partial pressure of CO$_2$ (pCO$_2$) has been increasing on average at a rate of 2–3 µatm per decade (Landschützer et al., 2018). Future increases in pCO$_2$ seasonality are expected, as marine CO$_2$ concentration ([CO$_2$]) will increase in response to increasing anthropogenic carbon emissions (McNeil and Sasse, 2016). Here we use seven different global coupled atmosphere–ocean–carbon cycle–ecosystem model simulations conducted as part of the Coupled Model Intercomparison Project Phase 5 (CMIP5) to study future projections of the pCO$_2$ annual cycle amplitude and to elucidate the causes of its amplification. We find that for the RCP8.5 emission scenario the seasonal amplitude (climatological maximum minus minimum) of upper ocean pCO$_2$ will increase by a factor of 1.5 to 3 over the next 60–80 years. To understand the drivers and mechanisms that control the pCO$_2$ seasonal amplification we develop a complete analytical Taylor expansion of pCO$_2$ seasonality in terms of its four drivers: dissolved inorganic carbon (DIC), total alkalinity (TA), temperature (T), and salinity (S). Using this linear approximation we show that the DIC and T terms are the dominant contributors to the total change in pCO$_2$ seasonality. To first order, their future intensification can be traced back to a doubling of the annual mean pCO$_2$, which enhances DIC and alters the ocean carbonate chemistry. Regional differences in the projected seasonal cycle amplitude are generated by spatially varying sensitivity terms. The subtropical and equatorial regions (40° S–40° N) will experience a $\approx$ 30–80 µatm increase in seasonal cycle amplitude almost exclusively due to a larger background CO$_2$ concentration that amplifies the T seasonal effect on solubility. This mechanism is further reinforced by an overall increase in the seasonal cycle of T as a result of stronger ocean stratification and a projected shoaling of mean mixed layer depths. The Southern Ocean will experience a seasonal cycle amplification of $\approx$ 90–120 µatm in response to the mean pCO$_2$-driven change in the mean DIC contribution and to a lesser extent to the T contribution. However, a decrease in the DIC seasonal cycle amplitude somewhat counteracts this regional amplification mechanism.

1 Introduction

Owing to its large chemical capacity to resist changes in [CO$_2$] (referred to as buffering capacity), the ocean has absorbed nearly half of the anthropogenic CO$_2$ produced by fossil fuel burning and cement production since the industrial revolution (Sabine et al., 2004). While the ocean's absorption of CO$_2$ lowers the atmospheric concentration, it also increases the ocean's [CO$_2$] and in turn lowers its buffering capacity. This leads to a reduction in the oceanic uptake of CO$_2$ and an intensification of the pCO$_2$ seasonal cycle (from now on referred to as δpCO$_2$) (Völker et al., 2002; McNeil and Sasse, 2016). In a recent key observational study by Landschützer et al. (2018), it was demonstrated that the δpCO$_2$ amplitude increased at a rate of $\approx$ 2–3 µatm per decade from 1982 to 2015.

The pCO$_2$ already experiences large seasonal fluctuations, which in some regions can reach up to 60 % above and below the annual mean pCO$_2$ (Takahashi et al., 2002). An intensification of the δpCO$_2$ amplitude could produce seasonal hypercapnia conditions (McNeil and Sasse, 2016), which together with increased [H$^+$] seasonality (Hagens and Middelburg, 2016; Kwiatkowski and Orr, 2018) and aragonite undersaturation events (Shaw et al., 2013; Hauri et al., 2015; Sasse et al., 2015) could expose marine life to harmful seawater conditions earlier than expected if considering only annual mean values. Moreover, a projected amplification of δpCO$_2$ might increase the net CO$_2$ uptake in some regions, such as the Southern Ocean, thereby further accelerating the decrease in the buffering capacity in that region (Hauck and Völker, 2015).

The pCO$_2$ seasonal amplitude is controlled mainly by seasonal changes in temperature (T) and biological activity together with upwelling changes that alter DIC concentrations. Usually, DIC and T changes work in opposite directions (Takahashi et al., 2002; Fay and McKinley, 2017; Sarmiento and Gruber, 2006). In subtropical regions higher pCO$_2$ values occur in summer when solubility decreases. In subpolar regions, pCO$_2$ increases in winter when waters upwell that are rich in DIC and when respiration of organic matter takes place. Decreased subpolar pCO$_2$ occurs in summer when primary productivity is higher and upwelling diminishes. Therefore, we find close relationships of δpCO$_2$ with the ocean's [CO$_2$], which controls chemical reactions, and with mean pCO$_2$, which moderates exchange with the atmosphere. Both factors are related by the solubility constant that depends on temperature and salinity.

Furthermore, the regional differences in the influence of temperature and biology on δpCO$_2$ are modulated by the ocean's buffering capacity. This is due to the ability of CO$_2$ to react with seawater to form bicarbonate [HCO$_3^-$] and carbonate [CO$_3^{2-}$], leaving only a small portion of dissolved carbon dioxide in the form of aqueous CO$_2$ ([CO$_2$(aq)]). [CO$_2$(aq)] together with carbonic acid ([H$_2$CO$_3$]) are defined as [CO$_2$]. Therefore, it is useful to define the total amount of carbon as DIC, which is the sum of the three carbon species ([HCO$_3^-$], [CO$_3^{2-}$], and [CO$_2$]). At current chemical conditions, most of the DIC is in the form of HCO$_3^-$, and therefore the buffering capacity is largely controlled by the CO$_3^{2-}$ capable of transforming CO$_2$ into bicarbonate through the reaction CO$_2$(aq) + CO$_3^{2-}$ + H$_2$O = 2HCO$_3^-$ (Zeebe and Wolf-Gladrow, 2001). The larger the buffering capacity, the larger the pCO$_2$ ability to resist changes in DIC. To quantify this capacity, we can introduce the sensitivity factor γ_{DIC}, which is inversely related to the buffering capacity, defined as $\gamma_{\mathrm{DIC}} = \partial \ln(p\mathrm{CO}_2)/\partial \mathrm{DIC}$, (Egleston et al., 2010). Other sensitivity factors are related to the total alkalinity (γ_{TA}), salinity (γ_{S}), and temperature (γ_{T}) changes and are defined in a similar way as $\partial \ln(p\mathrm{CO}_2)/\partial \mathrm{TA}$, $\partial \ln(p\mathrm{CO}_2)/\partial S$, and $\partial \ln(p\mathrm{CO}_2)/\partial T$, respectively. It is important to note that the

pCO$_2$ is highly sensitive to temperature due to two factors: first through solubility changes that account for 2 / 3 of the present-day temperature impact, and second through the dissociation constants that control the carbon system reactions (Sarmiento and Gruber, 2006).

While the mechanisms controlling the seasonal cycle of pCO$_2$ at present day are well documented, the future evolution of these drivers has not been fully elucidated. Current literature suggests that seasonal amplification is a consequence of an increase in the T and DIC contributions to δpCO$_2$ (Landschützer et al., 2018) and an increased sensitivity of the ocean to these variables (Fassbender et al., 2017).

The aim of our paper is to provide an in-depth analysis of the mechanisms controlling the future strength of δpCO$_2$ and its regional differences using seven CMIP5 global Earth system models. Our analysis focuses on 21st century evolution using the Representative Concentration Pathway 8.5 (RCP8.5) scenario. We give a comprehensive analysis of the projected evolution of the DIC, TA, T, and S contributions to pCO$_2$ seasonality. To achieve this goal, we derive explicit analytical expressions for pCO$_2$ sensitivities in terms of γ_{DIC}, γ_{TA}, γ_{T}, and γ_{S}, thereby extending previous work done by Egleston et al. (2010).

2 Methodology

2.1 CMIP5 models

For our analysis, pCO$_2$, DIC, TA, T, and S monthly mean output variables covering the period from 2006–2100 were obtained from future climate change simulations conducted with seven fully coupled Earth system models that participated in the Coupled Model Intercomparison Project, Phase 5 (CMIP5) (Taylor et al., 2012). The following models were selected based on data availability: CanESM2, CESM1-BGC, GFDL-ESM2M, MPI-ESM-LR, MPI-ESM-MR, HadGEM2-ES, and HadGEM2-CC (see the supplementary material of Hauri et al., 2015). For the purpose of this paper, we used the Representative Concentration Pathway 8.5 (RCP8.5) future climate change simulations (IPCC, 2013). The ocean's surface data sets were regridded onto a 1° × 1° grid using climate data operators (CDOs). The Arctic Ocean and the region poleward of 70° S are removed from the analyses because observational data for model validation are scarce.

2.2 Analysis of δpCO$_2$

To elucidate the underlying dynamical, thermodynamical, biological, and chemical processes controlling δpCO$_2$ we calculated a first-order Taylor series expansion of δpCO$_2$ in terms of its four drivers, DIC, TA, T, and S. While T and S are controlled only by physics, DIC and TA are controlled by physical, chemical, and biological processes. Throughout this paper we use salinity-normalized DIC and TA us-

ing a mean salinity of 35 psu. This effectively removes the concentration–dilution freshwater effect, following the procedure of Lovenduski et al. (2007). The salinity normalized variables are referred to as DIC$_s$ and TA$_s$, corresponding to DIC $\cdot S_0/S$ and TA $\cdot S_0/S$, respectively. The freshwater effect on DIC and TA is now included in the S term, renamed as S_{fw}. For the Taylor series expansion, each variable ($X =$ DIC, TA, T, and S) is decomposed into $X = \overline{X} + \delta X$. The term $\overline{X}$ represents the 21-year mean and δX denotes the seasonal cycle (calculated as the monthly mean deviation from the 21-year average). The Taylor expansion is then computed for an initial (2006–2026) and final (2080–2100) period. We use multi-decade means and eventually multi-model ensemble means to remove the effects of interannual variability. The full first-order series expansion is given by

$$\delta p\text{CO}_2 \approx \frac{\partial p\text{CO}_2}{\partial \text{DIC}}\Big|_{\overline{T},\overline{S}}^{\overline{\text{TA}},\overline{\text{DIC}}}\delta\text{DIC}_s + \frac{\partial p\text{CO}_2}{\partial \text{TA}}\Big|_{\overline{T},\overline{S}}^{\overline{\text{TA}},\overline{\text{DIC}}}\delta\text{TA}_s$$
$$+ \frac{\partial p\text{CO}_2}{\partial T}\Big|_{\overline{T},\overline{S}}^{\overline{\text{TA}},\overline{\text{DIC}}}\delta T + \frac{\partial p\text{CO}_2}{\partial S}\Big|_{\overline{T},\overline{S}}^{\overline{\text{TA}},\overline{\text{DIC}}}\delta S_{\text{fw}}. \quad (1)$$

Each term of the right-hand side of Eq. (1) represents the contribution from one of the four drivers of $\delta p\text{CO}_2$. The analytical expressions for the derivatives (without the salinity normalization) are given by the following.

$$\frac{\partial p\text{CO}_2}{\partial \text{TA}}\Big|_{\overline{T},\overline{S}}^{\overline{\text{TA}},\overline{\text{DIC}}} = \overline{p\text{CO}_2} \cdot \frac{-\overline{\text{Alk}_c}}{\overline{\text{DIC}} \cdot \Theta - \overline{\text{Alk}_c^2}} \quad (2)$$

$$\frac{\partial p\text{CO}_2}{\partial \text{DIC}}\Big|_{\overline{T},\overline{S}}^{\overline{\text{TA}},\overline{\text{DIC}}} = \overline{p\text{CO}_2} \cdot \frac{\Theta}{\overline{\text{DIC}} \cdot \Theta - \overline{\text{Alk}_c^2}}$$

$$\frac{\partial p\text{CO}_2}{\partial T}\Big|_{\overline{T},\overline{S}}^{\overline{\text{TA}},\overline{\text{DIC}}} = \overline{p\text{CO}_2} \cdot \frac{1}{\overline{\text{DIC}} \cdot \Theta - \overline{\text{Alk}_c^2}}$$
$$\left[\overline{\text{TA}_c} \cdot \left(\frac{\partial \text{Alk}_c}{\partial T} + \frac{\partial [\text{B(OH)}_4^-]}{\partial T} + \frac{\partial [\text{OH}^-]}{\partial T} \right) \right.$$
$$\left. -\Theta \cdot \frac{\partial (\text{DIC} - [\text{CO}_2])}{\partial T} \right] - \frac{\overline{p\text{CO}_2} \cdot}{\overline{K_0(T,S)}} \frac{\partial K_0(T,S)}{\partial T} \quad (3)$$

$$\frac{\partial p\text{CO}_2}{\partial S}\Big|_{\overline{T},\overline{S}}^{\overline{\text{TA}},\overline{\text{DIC}}} = \overline{p\text{CO}_2} \cdot \frac{1}{\overline{\text{DIC}} \cdot \Theta - \overline{\text{Alk}_c^2}}$$
$$\left[\overline{\text{Alk}_c} \cdot \left(\frac{\partial \overline{\text{Alk}_c}}{\partial S} + \frac{\partial [\text{B(OH)}_4^-]}{\partial S} + \frac{\partial [\text{OH}^-]}{\partial S} \right) \right.$$
$$\left. -\Theta \cdot \frac{\partial (\text{DIC} - [\text{CO}_2])}{\partial S} \right] - \frac{\overline{p\text{CO}_2} \cdot}{\overline{K_0(T,S)}} \frac{\partial K_0(T,S)}{\partial S} \quad (4)$$

Here, $\Theta = [\text{HCO}_3^-] + 4[\text{CO}_3^{2-}] + \frac{[\text{B(OH)}_4^-][\text{H}^+]}{(k_b + [\text{H}^+])} + [\text{H}^+] + [\text{OH}^-]$ and $\overline{\text{Alk}_c} = [\text{HCO}_3^-] + 2[\text{CO}_3^{2-}]$. The explicit T and S partial derivatives are given in the Supplement (Text S1). The first two derivatives coincide with the results of Egleston et al. (2010) and Hagens and Middelburg (2016), with the

exception of the sign of $[\text{OH}^-]$ in the Egleston et al. (2010) term S. To verify this approach we compared the sum of the Taylor expansion terms with the full simulated range of $\delta p\text{CO}_2$ from the model's output. The Taylor expansion reproduces the full seasonal cycle amplitude of the original climate model simulations well (Fig. S1 in the Supplement). The analytical expressions for temperature and salinity presented here are – to our knowledge – the first ones of their kind. Previously the calculation of these terms was based on the approximation given by Takahashi et al. (1993) or on numerical calculations.

To gain more insight into the processes causing the amplification of $\delta p\text{CO}_2$ we introduce a method based on a second Taylor series expansion described below. Equation (1) can be rewritten using the expressions for the sensitivities γ determined by the relation $\frac{1}{p\text{CO}_2}\frac{\partial p\text{CO}_2}{\partial X} = \gamma_X$. These sensitivities have been historically used to represent the percentage of change in $p\text{CO}_2$ per unit of DIC, TA, T, or S. With this notation, Eq. (1) can be expressed in the following way.

$$\delta p\text{CO}_2 \approx \overline{p\text{CO}_2} \cdot (\gamma_{\text{DIC}} \cdot \delta\text{DIC}_s + \gamma_{\text{TA}} \cdot \delta\text{TA}_s + \gamma_T$$
$$\cdot \delta T + \gamma_{S_{\text{fw}}} \cdot \delta S_{\text{fw}}) \quad (5)$$

Each term in Eq. (5) consists of three parts: $\overline{p\text{CO}_2}$, the sensitivity γ_X, and the corresponding seasonal cycle δX. To understand which component is the main driver for $\delta p\text{CO}_2$ changes, we perform a second Taylor expansion of the end of the century's $\delta p\text{CO}_2$ around the initial state of the system in 2006–2026.

To maximize mathematical clarity we will introduce some definitions: first, we introduce the symbol Δ to indicate the difference between the period 2080–2100 and 2006–2026. Therefore, the total future change in $\delta p\text{CO}_2$ is now referred to as $\Delta\delta p\text{CO}_2$. In the same manner, the total changes in sensitivities and seasonal cycles are written as $\Delta\gamma_{\text{DIC}_s}, \Delta\gamma_{\text{TA}_s}, \Delta\gamma_T, \Delta\gamma_{S_{\text{fw}}}$ and $\Delta\delta\text{DIC}_s, \Delta\delta\text{TA}_s, \Delta\delta T, \Delta\delta S_{\text{fw}}$, respectively. Finally, we introduce the vector X formed by the four variables DIC$_s$, TA$_s$, T, and S_{fw} as $\{X_0, X_1, X_2, X_3\} = \{\text{DIC}_s, \text{TA}_s, T, S\}$. With this notation, we can write an expansion of Eq. (5) of the final state of the system by 2080–2100 named X^{f} around the initial state $X^{\text{i}} = \{\text{DIC}_s{}^i, \text{TA}_s{}^i, T^i, S_{\text{fw}}^i\}$ by 2006–2026 as

$$\Delta\delta p\text{CO}_2 = \Delta\overline{p\text{CO}_2}\sum_{k=0}^{3} \gamma_{X_k}{}^i \cdot \delta X_k{}^i$$
$$+ \overline{p\text{CO}_2}^i\sum_{k=0}^{3} \Delta\gamma_{X_k} \cdot \delta X_k{}^i$$
$$+ \overline{p\text{CO}_2}^i\sum_{k=0}^{3} \gamma_{X_k}{}^i \cdot \Delta\delta X_k$$
$$+ \Delta\overline{p\text{CO}_2}\sum_{k=0}^{3} \Delta\gamma_{X_k} \cdot \delta X_k{}^i \text{(second-order terms)}$$

$$+ \Delta\overline{p\text{CO}_2} \sum_{k=0}^{3} \gamma_{X_k}{}^i \cdot \Delta\delta X_k$$

$$+ \overline{p\text{CO}_2}{}^i \sum_{k=0}^{3} \Delta\gamma_{X_k} \cdot \Delta\delta X_k, \tag{6}$$

where the first, second, and third terms represent the contributions to $\Delta\delta p\text{CO}_2$ due to changes in the mean $p\text{CO}_2$ ($\Delta\overline{p\text{CO}_2}$), the $p\text{CO}_2$ sensitivities ($\Delta\gamma_{X_k}$), and the seasonal cycles ($\Delta\delta X_k$), respectively; the fourth to sixth rows are the second-order terms. This method is similar to the one used by Landschützer et al. (2018).

3 Results and discussion

3.1 δpCO$_2$ amplification

Figure 1a shows the ensemble mean $\delta p\text{CO}_2$ amplitude (calculated as climatological maximum minus minimum) for the initial period 2006–2026. The values range from $\approx 98\,\mu$atm for the high latitudes (40–70° S, 40–60° N) to $\approx 60\,\mu$atm between 40° S and 40° N. The ensemble mean initial seasonal amplitude range is in good agreement with observational estimates calculated for the reference year 2005 (Takahashi et al., 2014b) and for the 1982–2015 period (Landschützer et al., 2017). The agreement between models and observations is remarkably good in the equatorial regions, but the initial amplitude is slightly overestimated in the middle and high latitudes (see Fig. S3 in the Supplement). The higher amplitude in models than observations is expected, as the initial period 2006–2026 already experienced an amplification compared to previous years. Moreover, Tjiputra et al. (2014) found that the ocean's $p\text{CO}_2$ historical trend is larger in models than observations when it is estimated in large-scale areas of the ocean. However, they found that model $p\text{CO}_2$ trends agree with observations when the trends are subsampled to the locations where the observations were taken, and therefore they do a good job of reproducing well-known time series. Moreover, differences are expected as Pilcher et al. (2015) suggested that CMIP5 models perform well in reproducing the seasonal cycle timing, but still show considerable errors in reproducing the seasonal amplitude of $p\text{CO}_2$ due to differences in the mechanisms represented in each model, especially in subpolar biomes.

By 2080–2100 the annual cycle amplitude attains values of ≈ 197 and $\approx 101\,\mu$atm in the high and middle to low latitudes, respectively (Fig. 1b). These seasonal variations correspond to 20 % and 18 % of annual $\overline{p\text{CO}_2}$ for the initial and final periods, respectively. Figure 1c shows that the global ocean $\delta p\text{CO}_2$ will intensify by a factor of 1.5 to 3 for the 2080–2100 period relative to the 2006–2026 reference period. Figure 1d shows the difference in amplitude ($\Delta\delta p\text{CO}_2$); this pattern differs from the ratio because the ratio overestimates the amplification in areas where the initial amplitude is lower than $\approx 10\,\mu$atm. McNeil and Sasse (2016) used observations

and a neural-network clustering algorithm to project that by the year 2100, the $\delta p\text{CO}_2$ amplitude in some regions could be up to 10 times larger than it was in the year 2000. Our mean amplification factor estimation agrees with the mean threefold amplification found for most of the ocean by McNeil and Sasse (2016). However, the high values in this previous study cannot be reproduced here, mainly because we consider 21-year average ratios instead of single-year ratios, which are strongly affected by interannual variability. Using observations, Landschützer et al. (2018) found an increase of $2.2\,\mu$atm per decade, which is smaller than our findings of a total $42\,\mu$atm increase by the end of the century between 40° S and 40° N and a global mean change of $81\,\mu$atm on the high latitudes. This difference is again possibly due to the higher mean $p\text{CO}_2$ values in models than observations.

The global ocean mean amplification factor of $\delta p\text{CO}_2$ roughly coincides with a doubling of $\overline{p\text{CO}_2}$ (Fig. 2). The direct relationship between these two is explained in Sect. 3.5. Figure 1e–h show the zonal mean of Fig. 1a–d; in general, towards the end of the century the $p\text{CO}_2$ amplifies more in high latitudes, but so does the standard deviation uncertainty among models. This regional pattern agrees with the observation-based findings of Landschützer et al. (2018), which show that high latitudes have already experienced a larger amplification than middle to low latitudes from 1982 to 2015. Furthermore, the same pattern is projected by CMIP5 models for the seasonal amplification of [H$^+$] by the end of the century (Kwiatkowski and Orr, 2018). This is expected from the near-linear relation between $p\text{CO}_2$ and [H$^+$]. These regional differences in amplification for $p\text{CO}_2$ can be explained in terms of the relative magnitudes and the phases between the DIC, TA, T, and S contributions, which are explained in subsequent sections.

3.2 Present and future drivers of δpCO$_2$

To understand the driving factors of $\delta p\text{CO}_2$ and its spatiotemporal differences, we split $\delta p\text{CO}_2$ into the four different contributions from DIC$_s$, TA$_s$, T, and S_{fw} for the initial and final periods, following Eq. (1). The results are shown in Fig. 3. For most of the ocean, the ensemble mean estimated contributions from DIC$_s$ and T to the present-day $\delta p\text{CO}_2$ are in good agreement with the data-based estimates of Takahashi et al. (2014b) and Landschützer et al. (2017), particularly in the equatorial regions (see Fig. S3 in the Supplement). However, our T and DIC contributions are slightly larger in middle and high latitudes for the same reasons the $p\text{CO}_2$ seasonal amplitude is overestimated (see Sect. 3.1). Also, differences arise between our DIC$_s$ contribution and the observation-based so-called "nonthermal" contribution because the nonthermal contribution also includes the total alkalinity and salinity effects. Nonetheless, between 40° S and 40° N our ensemble mean shows that $\delta p\text{CO}_2$ is dominated by changes in temperature that control CO$_2$ solubility, which decreases in summer, enhancing $p\text{CO}_2$; this is in
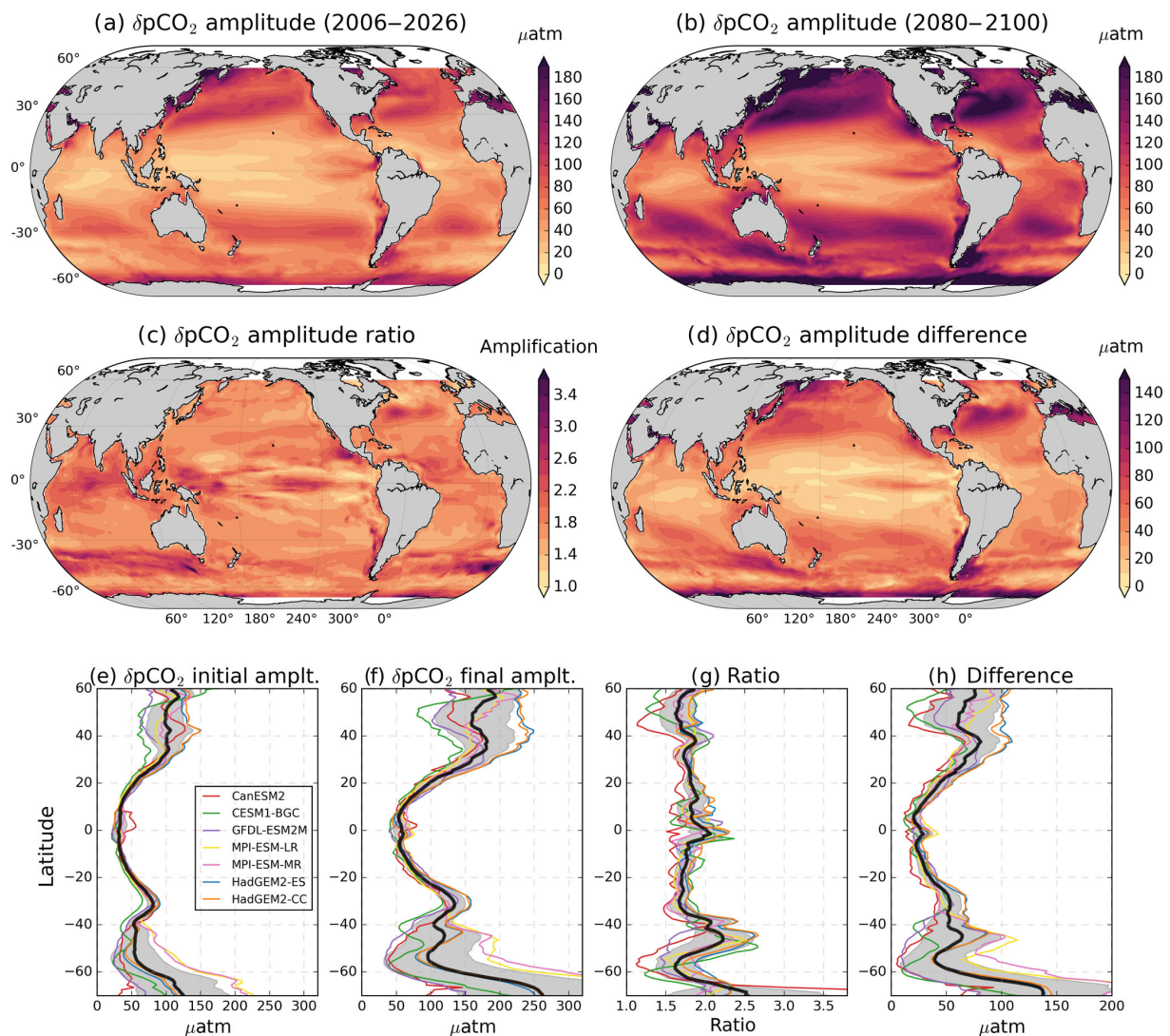
Figure 1. RCP8.5 ensemble mean pCO$_2$ seasonal cycle amplitude. Amplitude is calculated as climatology maximum minus minimum for **(a)** initial (2006–2026) and **(b)** final (2080–2100) periods. Initial and final climatologies were calculated as the monthly deviation from the respective 21-year period mean. **(c, d)** The ratio and difference between the δpCO$_2$ amplitudes for 2080–2100 and 2006–2026, respectively. **(e)**–**(h)** The zonal means of **(a)**–**(d)**, respectively, with the individual models shown as colored lines and the ensemble mean overlaid in black. Gray shading represents 1 standard deviation across the models.

agreement with observations. The Southern Ocean is controlled by DIC, which responds to changes in upwelling and phytoplankton blooms. Both mechanisms act together to decrease (increase) DIC in summer (winter) (Sarmiento and Gruber, 2006).

The models show that the δpCO$_2$ in the 40° N to 60° N band is controlled by T, which disagrees with the abovementioned observations that show a non-temperature dominance in this band. The difference between models and observations arises from two regions: the North Atlantic basin and the northwestern Pacific, specifically near the Oyashio current and the outflows from the Sea of Okhotsk (see Fig. S3 in the Supplement). Most models show a T dominance in

the North Atlantic basin; only CESM1-BGC and GFDL-ESM2M show a DIC dominance (see Fig. S4 in the Supplement). The North Atlantic is one of the major sinks of anthropogenic CO$_2$; however, some models fail to estimate its uptake capacity (Goris et al., 2018). Goris et al. (2018) found that models with an efficient carbon sequestration present a DIC-dominated pCO$_2$ seasonal cycle in the North Atlantic, but models with low anthropogenic uptake show a T dominance in this region. In the northwestern Pacific, Mckinley et al. (2006) found that coarse models are not able to capture the intricate oceanographic features of this area, and therefore the pCO$_2$ seasonality is not well captured.
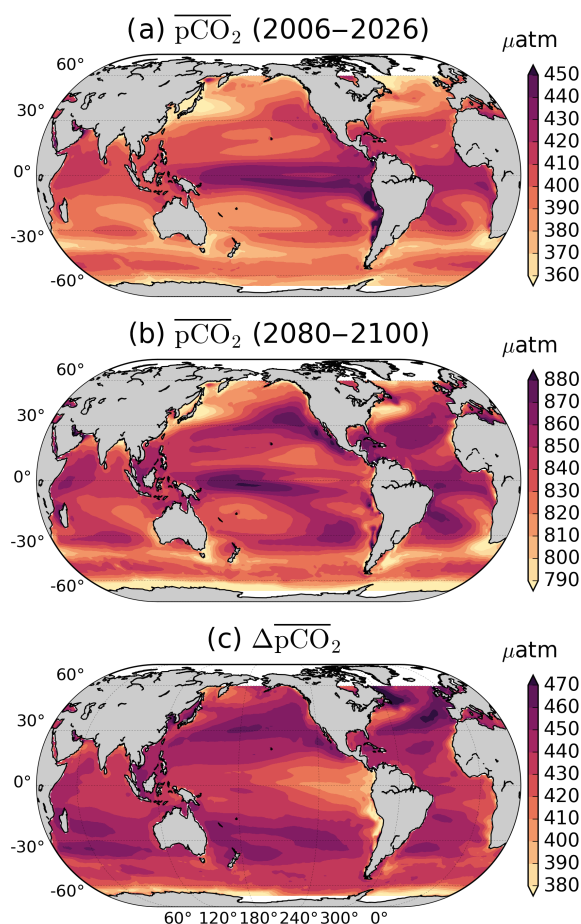
Figure 2. RCP8.5 ensemble mean $\overline{pCO_2}$ by **(a)** 2006–2026 and **(b)** 2080–2100. **(c)** Difference between 2080–2100 and 2006–2026. The North Atlantic and subpolar gyres show the largest difference between initial and final periods. The scale is different in each plot to enhance regional features.

Towards the end of the century (Fig. 3, right column), the amplification of δpCO_2 is caused by an increase in the DIC_s and T contributions and to a lesser extent due to TA_s and S_{fw}. Only in the high latitudes does the TA_s contribution reinforce the DIC_s effect. The δDIC_s and δT relative phase and magnitude play an important role in causing regional differences of future δpCO_2. For example, between 40 and 60°, we find a lower amplification factor than at 30–40° in both hemispheres (Fig. 1c), contrary to what we expected from the general observed larger amplification at higher latitudes. In this band of lower amplification, the warm water from subtropical regions meets the nutrient-rich water from the subpolar regions, but the DIC_s and T effects are almost 6 months out of phase, and therefore their cancellation is larger than in the 30–40° latitude band where, for example, in the North Atlantic, there is 9-month phase difference between the two contributions. A clear illustration of this phase effect is found in the Supplement (Fig. S5).

In the Southern Ocean there is a shift in the maximum δpCO_2 occurring from August–September to March–April (Fig. 3, last row). This shift is generated because the T contribution gains importance over DIC_s due to a reduction of δDIC_s magnitude at the same time that δT increases (Fig. 5). In the equatorial Pacific region (Fig. 5), T dominates over DIC_s but both contributions are small due to their low seasonality. Therefore, this region will experience a low amplification in δpCO_2. In this region some models underestimate the pCO_2 trend (Tjiputra et al., 2014), and therefore the seasonal amplification might be underestimated too. In the following sections we conduct further analysis by decomposing each contribution as the result of three factors: the mean pCO_2 ($\overline{pCO_2}$), the regional pCO_2 sensitivities (γ_{DIC}, γ_{TA}, γ_T, and $\gamma_{S_{fw}}$), and the seasonal cycles (δDIC_s, δTA_s, δT, and δS_{fw}) as determined in Eq. (5).

3.3 Future pCO_2 sensitivities

The γ_{DIC} and γ_{TA} are projected to increase by the end of the century due to a lower ocean buffering capacity produced by increasing temperature and larger background concentrations of DIC (Fassbender et al., 2017). This agrees with our results shown in Fig. 4, which shows that all regions will experience an increase in γ_{DIC} and γ_{TA}. Lower buffer factors (higher sensitivities factors) are found in regions where DIC and TA have similar values, and they will decrease (increase) as the DIC / TA ratio in the oceans increases (Egleston et al., 2010). The alkalinity sensitivity is negative, as pCO_2 decreases with increasing alkalinity, but we show here the negative γ_{TA} for better comparison. γ_{TA} will increase (with negative values) more than the DIC sensitivity. However, seasonal changes in open-ocean TA_s are small, and therefore the total contribution of alkalinity in our analysis is negligible compared to the DIC_s and T contributions. $\gamma_{S_{fw}}$ decreases everywhere except in the Western Pacific Warm Pool. In this region $\gamma_{S_{fw}}$ increases, probably due to future changes in precipitation that enhance the freshwater effect. In Fig. 4, the sensitivities (γ) are expressed as a percentage change in pCO_2 per unit in DIC, TA, T, and S, respectively. This follows the approach of Takahashi et al. (1993); however, in their paper the authors compute the Revelle factor, which is related to γ_{DIC} as $R = DIC \cdot \gamma_{DIC}$. To illustrate the meaning of the sensitivities, we will focus on the subtropical North Pacific in the 15–40° N latitudinal band. In this region γ_{DIC} indicates an average 0.6 % change in pCO_2 per unit of DIC in 2006–2026. Therefore, for a δDIC_s seasonal cycle amplitude of $40 \, \mu mol \, kg^{-1}$ and $\overline{pCO_2} \approx 400 \, \mu atm$, the total δpCO_2 amplitude equals $96 \, \mu atm$. Following the same reasoning, by 2080–2100, γ_{DIC} increases to 0.7 % and δDIC_s decreases to $30 \, \mu mol \, kg^{-1}$; therefore, for a $\overline{pCO_2}$ equal to $800 \, \mu atm$, the δpCO_2 amplitude due to δDIC amounts to $168 \, \mu atm$.

Temperature sensitivity has been experimentally determined by Takahashi et al. (1993), who found a value of 0.0423, meaning that pCO_2 changes by about 4 % for ev-
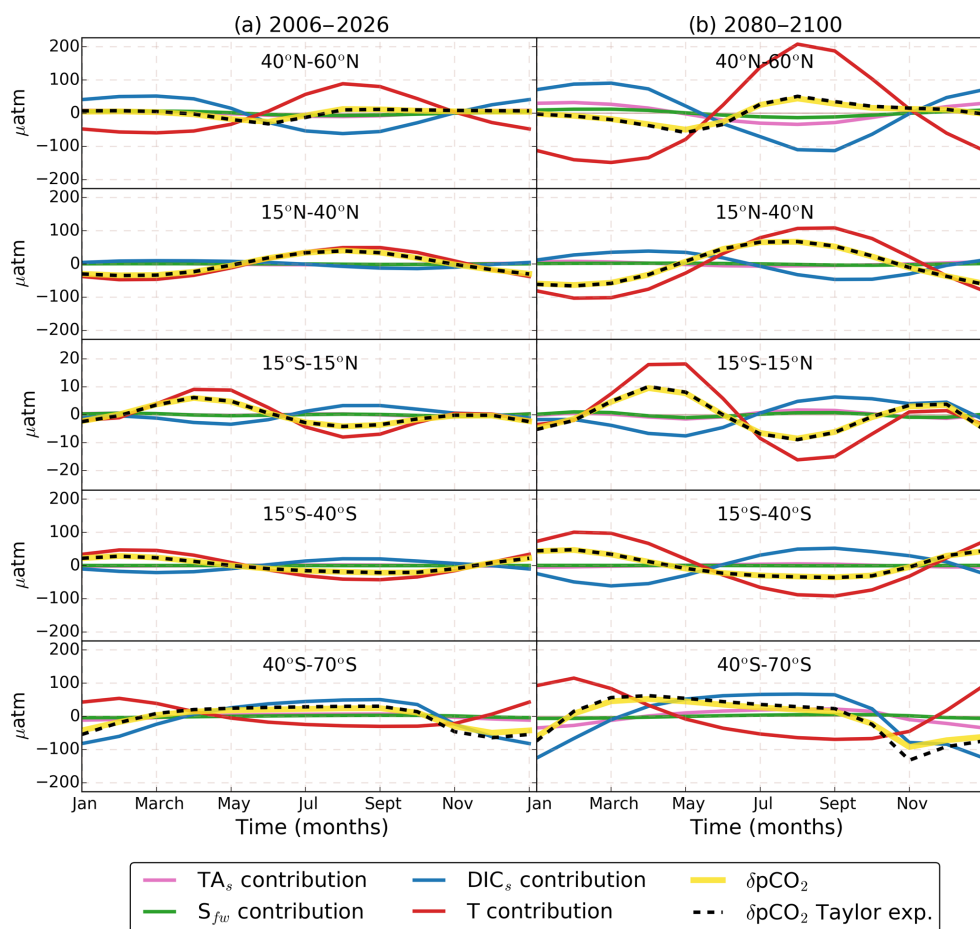
Figure 3. RCP8.5 ensemble mean seasonal cycle (δpCO$_2$) and its Taylor decomposition. Colored lines indicate the contributions of DIC$_s$ (blue), TA$_s$ (pink), T (red), and S_{fw} (green) to δpCO$_2$ reconstructed from its Taylor decomposition (Eq. 1; dashed black). δpCO$_2$ calculated from monthly pCO$_2$ (solid yellow) is shown for comparison with the Taylor expansion. Column **(a)** shows the period 2006–2026 and column **(b)** shows the period 2080–2100. Each row represents the global zonal average for a different latitudinal band. Temperature dominates all latitudes except the Southern Ocean. In the 40–60° N band, T contribution is largely compensated for by DIC. The TA$_s$ and S_{fw} effects are rather small in all latitudes.

ery °C. This value agrees with our global mean ensemble estimate of 0.0428. However, our analytical expression of γ_T shows that this value varies regionally and, for reasons unknown to us, it might decrease in the future to a global mean value of 0.0415 (Fig. 4c, third column). The T sensitivity is larger in colder regions and lower in the warmer tropics; however, colder regions will experience a larger reduction in γ_T, which locally prevents a larger amplification of the T contribution to δpCO$_2$. In the next section we show that the T seasonality is projected to increase in high latitudes, strengthening the T contribution.

3.4 Future δDIC$_s$, δTA$_s$, δT, and δS_{fw}

Towards the end of the century, the global mean amplitude of δDIC$_s$ is projected to decrease by $\approx$ 26 %–28 % in the high latitudes (Fig. 5a), according to all the CMIP5 Earth system model simulations used here. In the middle to low latitudi-

nal band there is no agreement between models; while some show an increase, others project a decrease in amplitude. As suggested by Landschützer et al. (2018), the larger decrease in the Southern Ocean may be the result of changes in the shallow overturning circulation that prevent CO$_2$ accumulation in this region. This reduction may be counteracted by the predicted increase in productivity owing to a suppression of light and temperature limitations (Steinacher et al., 2010; Bopp et al., 2013).

According to the CMIP5 models, most of the ocean is projected to experience a slight increase in δT, as shown in Fig. 5b. All models show a slight increase in δT; only one model showed a slightly decrease in the southern region, and two models showed a decrease in the equatorial region during October to December. It is important to note that Fig. 5 shows the seasonal values with the mean T removed. Therefore, when considering the positive T trends, the absolute
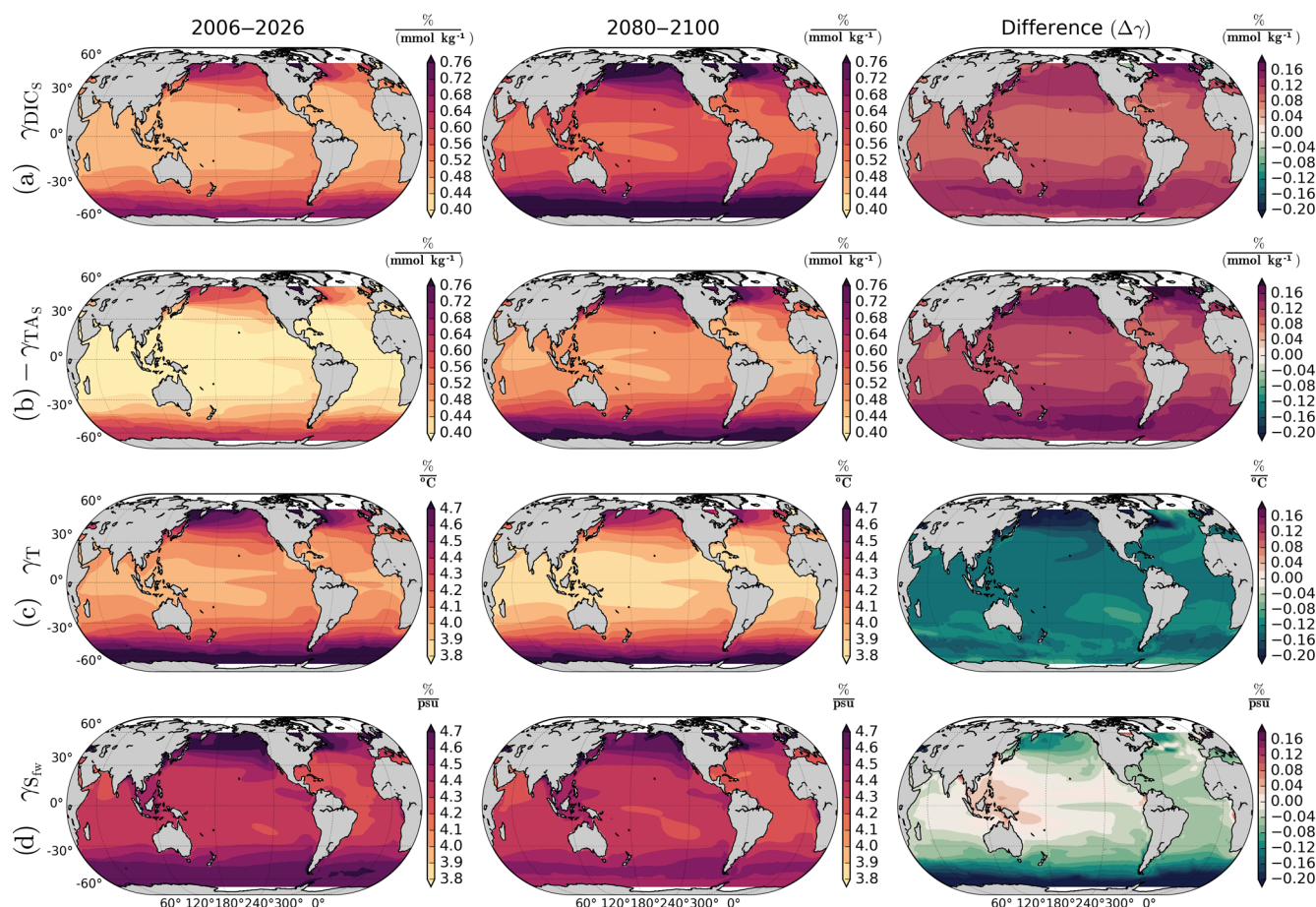
Figure 4. RCP8.5 ensemble mean pCO$_2$ sensitivities for DIC$_s$ (row **a**), TA$_s$ (row **b**), T (row **c**), and S_{fw} (row **d**). Row (**b**) shows the negative γ_{TA}. The first and second columns show the sensitivities by 2006–2026 and 2080–2100, respectively. The third column shows the difference between 2080–2100 and 2006–2026 sensitivities. High latitudes show the largest difference between initial and final periods. While DIC$_s$ and TA$_s$ sensitivities increase, the T and S_{fw} sensitivities decreases, except in the Western Pacific Warm Pool, where $\gamma_{S_{fw}}$ increases.

summer values show an increase and the absolute winter values a decrease. This agrees with the results of Alexander et al. (2018), who showed that models project a seasonal intensification of T with larger warm extremes and reduced cold extremes. The authors attributed the T seasonality intensification to an increased oceanic stratification and an overall shoaling of the mixed layer depth, which confines seasonal changes in a reduced volume of water, producing larger changes at the surface. They also showed that the intensification trends are stronger in summer than winter, as the mixed layer depth is shallower in summer. Moreover, ice-covered regions will experience the largest increase in T seasonality due to the loss of sea ice because the ice melting and freezing moderates the surface water temperature seasonality (Carton et al., 2015).

The TA seasonality is also projected to increase in the high latitudes according to all models, except CESM1-BGC, which shows a decrease. For δS (see Fig. S6 in the Supplement) there is no agreement among the different CMIP5

models, except in the Southern Ocean where all the models show a slight decrease. Kwiatkowski and Orr (2018) demonstrated that the seasonality of the drivers is important to determine future changes in [H$^+$] seasonality. In the same fashion, our results show that the four δpCO$_2$ drivers present changes in seasonality, and in particular δDIC$_s$ and δT changes are important to explain future projections of the δpCO$_2$ amplitude. The increase in δT enhances the δpCO$_2$ amplification, and the reduction of δDIC$_s$ in the Southern Ocean locally prevents a larger amplification.

3.5 Regional dominant factors

To identify the main cause of the δpCO$_2$ amplification we use the Taylor series expansion method. With this method we consider the system's final state (δpCO$_2$ by 2080–2100) as a perturbation of the initial state (δpCO$_2$ by 2006–2026), as shown in Eq. (6). The expansion is done in three groups of variables: the seasonal cycles of DIC$_s$, TA$_s$, T, and S (δX), the sensitivities of pCO$_2$ to the same four variables (γ_x), and
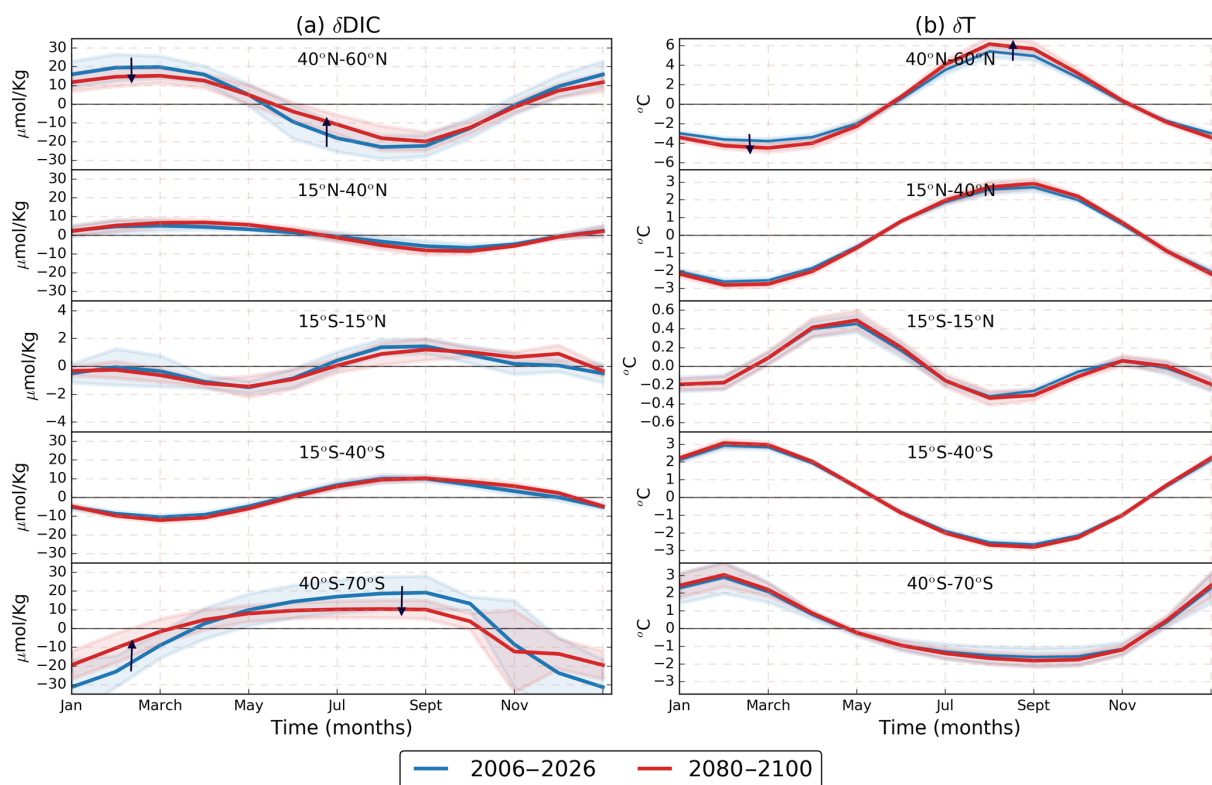
Figure 5. RCP8.5 ensemble zonal mean seasonal cycles of **(a)** $\delta\mathrm{DIC_s}$ and **(b)** δT for different latitudinal bands. Blue lines represent the 2006–2026 period, depicted for comparison with the 2080–2100 period shown by red lines. Different panels represent different latitudinal sections. Black arrows point out that while the T seasonal cycle is projected to increase in most of the ocean, global $\mathrm{DIC_s}$ is projected to decrease. The shading represents 1 standard deviation across the models. It is important to note that the scale is different for some of the latitudinal bands.

the mean $p\mathrm{CO_2}$ ($\overline{p\mathrm{CO_2}}$). Therefore, each term of the expansion represents how much of the total $\delta p\mathrm{CO_2}$ change (indicated by $\Delta\delta p\mathrm{CO_2}$ and calculated as the 2080–2100 value minus the 2006–2026 value) is due to the change in each of these factors. We also add the second-order terms that come from their combination. The results are shown in Fig. 6a and they indicate that the leading cause of the $\delta p\mathrm{CO_2}$ amplification is the change in $\overline{p\mathrm{CO_2}}$ ($\Delta\overline{p\mathrm{CO_2}}$), which confirms previous findings by Landschützer et al. (2018).

It is important to note that our linear Taylor expansion approach neglects one aspect of the highly nonlinear carbonate chemistry of the ocean: it assumes $\overline{p\mathrm{CO_2}}$ and the sensitivities as independent variables and therefore does not include the positive feedback between larger $\overline{p\mathrm{CO_2}}$ and increasing γ_{DIC} (decreasing buffering capacity). Hence in the following, we use changes in $\overline{p\mathrm{CO_2}}$ and changes in seawater carbonate chemistry synonymously, overall resulting in an enhanced response of $\delta p\mathrm{CO_2}$ to seasonal changes in DIC, TA, T, and S.

Considering regional differences, we note that amplification increases as we move poleward in spite of decreasing $\Delta\overline{p\mathrm{CO_2}}$ (see Figs. 1 and 2). This characteristic geographical pattern of stronger high-latitude amplification is the result of larger present-day sensitivities ($\gamma_{\mathrm{DIC_s}}$, γ_T) and seasonal am-

plitudes ($\delta\mathrm{DIC_s}$, δT) in the high latitudes that amplify the effect of $\Delta\overline{p\mathrm{CO_2}}$ even when its value is small compared to other regions (see Eq. 6, first row term). Some exceptions can be found south of Greenland and near the subtropical gyres, where $\Delta\overline{p\mathrm{CO_2}}$ reaches higher values and therefore also presents large amplification. We also found spatial differences on smaller scales; for example, the western equatorial Pacific presents lower initial $\delta p\mathrm{CO_2}$ and amplification than the eastern equatorial Pacific (see Fig. 1). This is because the eastern side of the basin has larger $\mathrm{DIC_s}$ and T contributions than the western side (see Fig. S2) as a consequence of the upwelling of cold, $\mathrm{CO_2}$-rich waters in the east, which lower the buffering capacity and induce larger $\delta p\mathrm{CO_2}$ amplitude due to the seasonal effects of productivity and solubility (Valsala et al., 2014).

To further disentangle which of the two main drivers ($\mathrm{DIC_s}$ or T) is most affected by $\Delta\overline{p\mathrm{CO_2}}$, we decomposed the $\mathrm{DIC_s}$ and T contributions into their sensitivity, seasonal cycle, and $\overline{p\mathrm{CO_2}}$ components. Figure 6b shows the total DIC and T components together with the $\Delta\overline{p\mathrm{CO_2}}$ and seasonal cycle effects on them. The effects from the sensitivities are not depicted, as they only play a minor role. Only the $\Delta\gamma_{\mathrm{DIC}}$ term gains importance in the Southern Ocean (not shown).
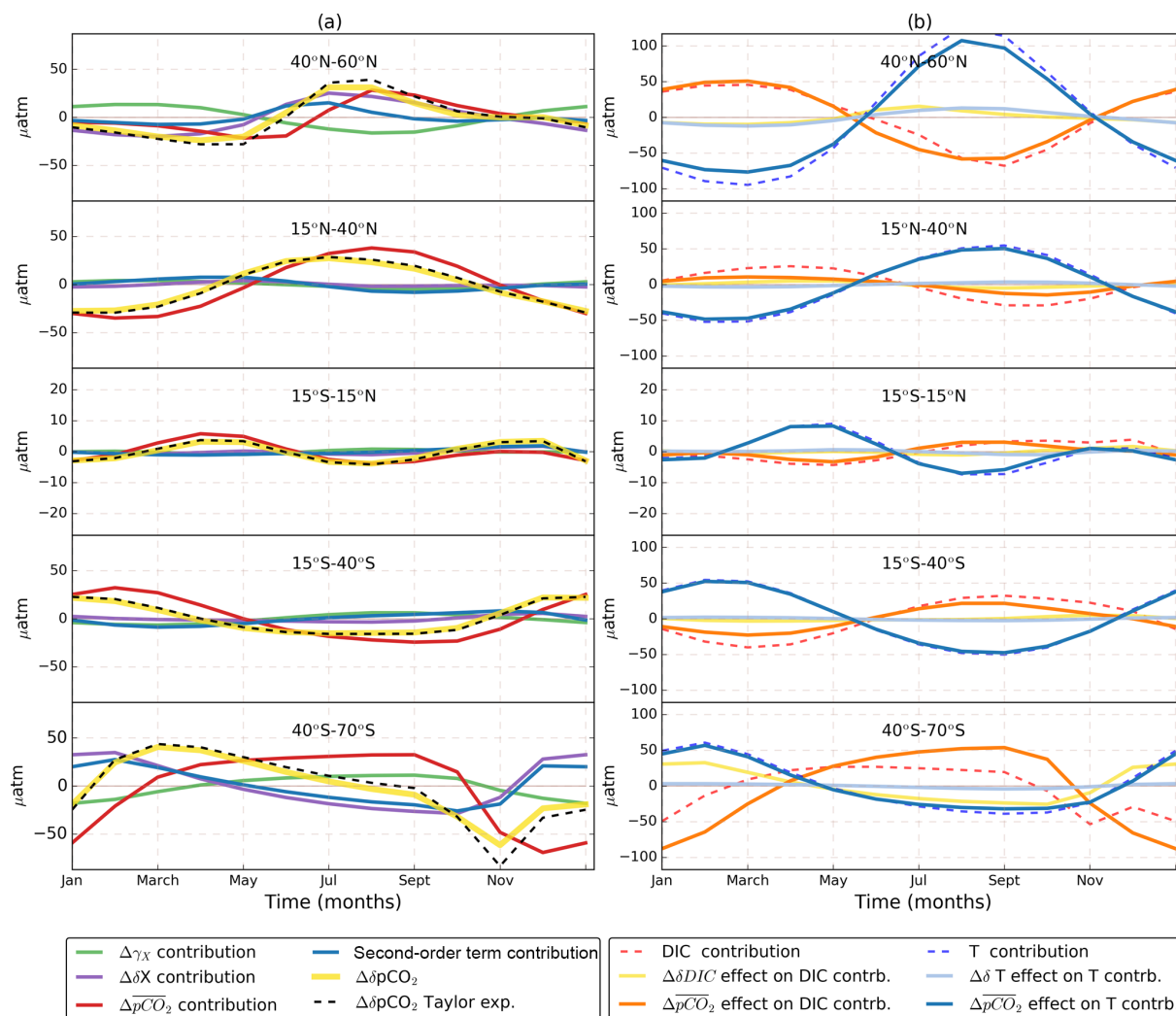
Figure 6. Contribution of seasonalities, sensitivities, and mean pCO$_2$ changes to $\Delta \delta p$CO$_2$. **(a)** Time series for the terms of Eq. (6) for different latitudinal bands. The Δ symbol represents the total century change calculated as the 2080–2100 value minus the 2006–2026 value. The total change in seasonal pCO$_2$ ($\Delta \delta p$CO$_2$) is depicted as a dashed black. This change is decomposed into changes in seasonalities ($\Delta \delta X$, purple), sensitivities ($\Delta \gamma_X$, green), mean pCO$_2$ ($\Delta \overline{p\text{CO}_2}$, red), and second-order terms (blue) summed over the four variables that control pCO$_2$ (DIC, TA, T and S). For comparison with the expansion, $\Delta \delta p$CO$_2$ is calculated from model output (yellow). Column **(b)** shows the total change in DIC (dashed red) and T (dashed blue) contributions. Also shown are two components of the total change in these contributions: the $\Delta \overline{p\text{CO}_2}$ effect on the DIC (solid orange) and T (solid blue) contributions and the $\Delta \delta$DIC (yellow) and $\Delta \delta T$ (light blue) effects. In column **(a)**, the δpCO$_2$ change follows the $\Delta \overline{p\text{CO}_2}$ effect. Column **(b)** shows that, actually, the leading cause of amplification is the $\Delta \overline{p\text{CO}_2}$ effect on the T contribution. It is important note the different scale between column **(a)** and **(b)**. Also, the scale was reduced in the 15° S–15° N region to highlight its features.

In most of the ocean, the $\Delta \overline{p\text{CO}_2}$ effect on T contribution is the leading cause of amplification. This effect is the result of seasonal solubility changes acting over a larger [CO$_2$] (Gorgues et al., 2010). In the northern high latitudes, an increase in δT reinforces the amplification. In general, the $\Delta \delta T$ contribution gains importance as we move poleward in both hemispheres and therefore the second-order terms originating from $\Delta \overline{p\text{CO}_2} \cdot \Delta \delta T$ also reinforce the amplification. Interestingly, in the high latitudes, the amplification through

second-order terms is as important as the change in the seasonality of the drivers.

The Southern Ocean is an exception to the T dominance; in this region the $\Delta \overline{p\text{CO}_2}$ effect on the DIC$_s$ contribution dominates, and the regional amplification is reinforced by low values of the mean buffering capacity (high γ_{DIC_s}). This result agrees with the findings of Hauck and Völker (2015). In this area the amplification is counteracted by a reduction in δDIC$_s$.

4   Conclusions

In this study, we used output from seven CMIP5 global models, subjected to the RCP8.5 radiative forcing scenarios, to provide a comprehensive analysis of the characteristics and drivers of the intensification of the seasonal cycle of pCO$_2$ between present (2006–2026) and future (2080–2100) conditions. By 2080–2100 the δpCO$_2$ will be 1.5–3 times larger compared to 2006–2026. The projected amplification by the Earth system models and the possible causes of it are consistent with observation-based amplification for the period from 1982 to 2015 (Landschützer et al., 2018). However, the models slightly overestimate the present-day amplification, probably due to the larger pCO$_2$ trends in models than observations (Tjiputra et al., 2014).

The models confirm the well-established mechanisms controlling present-day δpCO$_2$ (Takahashi et al., 2002; Sarmiento and Gruber, 2006; Fay and McKinley, 2017). DIC$_s$ and T contributions are the main counteracting terms dominating the seasonal evolution of δpCO$_2$. Furthermore, the models show that under future conditions the controlling mechanisms remain unchanged. This result confirms the findings of Landschützer et al. (2018) that identified the same regional controlling mechanism for the past 30 years. The relative role of the DIC and T terms is regionally dependent. High latitudes and upwelling regions, such as the California current system and the coast of Chile, are dominated by DIC$_s$ and the temperate low latitudes are driven by T. Only in the North Atlantic and northwestern Pacific do the models show a dominance of thermal effects over nonthermal effects, which is in disagreement with observations. This further illustrates the urgent need for models to accurately represent regional oceanographic features to accurately reproduce the δpCO$_2$ characteristics.

In agreement with Landschützer et al. (2018), the model projections towards the end of this century also demonstrate that the global amplification of δpCO$_2$ is due to the overall long-term increase in anthropogenic CO$_2$. A higher oceanic background CO$_2$ concentration enhances the effect of T-driven solubility changes on δpCO$_2$ and alters the seawater carbonate chemistry, also enhancing the DIC seasonality effect. The spatial differences of δpCO$_2$ amplification, however, are determined by the regional sensitivities and seasonality of pCO$_2$ drivers. For example, polar regions show larger sensitivity to DIC and T and larger seasonal cycles of DIC and T. Therefore, these areas present a strong enhancement of δpCO$_2$ in spite of smaller changes in mean pCO$_2$.

Moreover, the pCO$_2$ seasonal cycle amplitude depends on the relative magnitude and phase of the contributions. The models ensemble mean reproduces the highly effective compensation of DIC$_s$ and T contributions when they are 6 months out of phase, confirming previous studies (Takahashi et al., 2002; Landschützer et al., 2018). The compensation of DIC and T prevents a larger amplification of δpCO$_2$, even when both contributions are largely amplified.

The amplification of the TA and S contributions has a small impact on δpCO$_2$ in most regions, except in the high latitudes at which the TA contribution complements the DIC one, enhancing the nonthermal effect in this region.

The use of Earth system models allowed us to state the importance of including future changes in driver seasonalities for future δpCO$_2$ projections. The T seasonality is projected to increase in most of the ocean basins, thereby reinforcing the δpCO$_2$ amplification. The δT increase is consistent with an increase in stratification that will confine the seasonal changes in net heat fluxes to a shallower mixed layer (Alexander et al., 2018). The DIC$_s$ seasonality decreases in some cold areas and its reduction prevents a larger amplification. For the sensitivities, while γ_{DIC} increases, γ_T decreases. The latter phenomenon needs further study.

The increasing amplitude of δpCO$_2$ might have implications for the net air–sea flux of CO$_2$, in particular in regions where there is an imbalance between winter and summer values (Gorgues et al., 2010). Examples of such behavior can be found in the Southern Ocean (between 50 and 60° S) (Takahashi et al., 2014a) and in the latitude band from 2–40° in both hemispheres (Landschützer et al., 2014). Moreover, seasonal events of high pCO$_2$ could have an impact on acidification, aragonite undersaturation events (Sasse et al., 2015), and hypercapnia conditions (McNeil and Sasse, 2016). Therefore, understanding the drivers of future δpCO$_2$ may help to better assess the response of marine ecosystems to future changes in carbonate chemistry. Finally, our complete analytical expansion of δpCO$_2$ in terms of its four variables provides a practical tool to accurately and quickly diagnose temperature and salinity sensitivities from observational or modeling data sets.

The Supplement related to this article is available online at https://doi.org/10.5194/bg-15-5315-2018-supplement.

References

Alexander, M. A., Scott, J. D., Friedland, K. D., Mills, K. E., Nye, J., Pershing, A. J., and Thomas, A. C.: Projected sea surface temperatures over the 21st century: Changes in the mean, variability and extremes for large marine ecosystem regions of Northern Oceans, Elem. Sci. Anth., 6, 9, https://doi.org/10.1525/elementa.191, 2018.

Bopp, L., Resplandy, L., Orr, J. C., Doney, S. C., Dunne, J. P., Gehlen, M., Halloran, P., Heinze, C., Ilyina, T., Séférian, R., Tjiputra, J., and Vichi, M.: Multiple stressors of ocean ecosystems in the 21st century: projections with CMIP5 models, Biogeosciences, 10, 6225–6245, https://doi.org/10.5194/bg-10-6225-2013, 2013.

Carton, J. A., Ding, Y., and Arrigo, K. R.: The seasonal cycle of the Arctic Ocean under climate change, Geophys. Res. Lett., 42, 7681–7686, 2015.

Egleston, E. S., Sabine, C. L., and Morel, F. M. M.: Revelle revisited: Buffer factors that quantify the response of ocean chemistry to changes in DIC and alkalinity, Global Biogeochem. Cy., 24, GB1002, https://doi.org/10.1029/2008GB003407, 2010.

Fassbender, A. J., Sabine, C. L., and Palevsky, H. I.: Nonuniform ocean acidification and attenuation of the ocean carbon sink, Geophys. Res. Lett., 44, 8404–8413, 2017.

Fay, A. R. and McKinley, G. A.: Correlations of surface ocean pCO$_2$ to satellite chlorophyll on monthly to interannual timescales, Global Biogeochem. Cy., 31, 436–455, 2017.

Gorgues, T., Aumont, O., and Rodgers, K. B.: A mechanistic account of increasing seasonal variations in the rate of ocean uptake of anthropogenic carbon, Biogeosciences, 7, 2581–2589, https://doi.org/10.5194/bg-7-2581-2010, 2010.

Goris, N., Tjiputra, J., Olsen, A., Schwinger, J., Lauvset, S. K., and Jeansson, E.: Constraining projection-based estimates of the future North Atlantic carbon uptake, J. Climate, 31, 3959–3978, 2018.

Hagens, M. and Middelburg, J. J.: Attributing seasonal pH variability in surface ocean waters to governing factors, Geophys. Res. Lett., 43, 12528–12537, 2016.

Hauck, J. and Völker, C.: Rising atmospheric CO$_2$ leads to large impact of biology on Southern Ocean CO$_2$ uptake via changes of the Revelle factor, Geophys. Res. Lett., 42, 1459–1464, 2015.

Hauri, C., Friedrich, T., and Timmermann, A.: Abrupt onset and prolongation of aragonite undersaturation events in the Southern Ocean, Nat. Clim. Change, 6, 172–176, 2015.

IPCC: IPCC Climate Change 2013: The Physical Science Basis, Contribution of Working Group I to the Fifth Assessment Report of the Intergovernmental Panel on Climate Change, 2013.

Kwiatkowski, L. and Orr, J.: Diverging seasonal extremes for ocean acidification during the twenty-first century, Nat. Clim. Change, 8, 141–145, 2018.

Landschützer, P., Gruber, N., Bakker, D. C. E., and Schuster, U.: Recent variability of the global ocean carbon sink, Global Biogeochem. Cy., 28, 927–949, 2014.

Landschützer, P., Gruber, N., and Bakker, D.: An updated observation-based global monthly gridded sea surface pCO$_2$ and air-sea CO$_2$ flux product from 1982 through 2015 and its monthly climatology (NCEI Accession 0160558), Version 2.2. NOAA National Centers for Environmental Information, Dataset, https://doi.org/10.7289/V5Z899N6, 2017.

Landschützer, P., Gruber, N., Bakker, D. C. E., Stemmler, I., and Six, K. D.: Strengthening seasonal marine CO$_2$ variations due to increasing atmospheric CO$_2$, Nat. Clim. Change, 8, 146–150, 2018.

Lovenduski, N. S., Gruber, N., Doney, S. C., and Lima, I. D.: Enhanced CO$_2$ outgassing in the Southern Ocean from a positive phase of the Southern Annular Mode, Global Biogeochem. Cy., 21, GB2026, https://doi.org/10.1029/2006GB002900, 2007.

Mckinley, G. A., Takahashi, T., Buitenhuis, E., Chai, F., Christian, J. R., Doney, S. C., Jiang, M., Lindsay, K., Moore, J. K., Quere, C. L., Lima, I., Murtugudde, R., Shi, L., and Wetzel, P.: North Pacific carbon cycle response to climate variability on seasonal to decadal timescales, J. Geophys. Res., 111, C07S06, https://doi.org/10.1029/2005JC003173, 2006.

McNeil, B. I. and Sasse, T. P.: Future ocean hypercapnia driven by anthropogenic amplification of the natural CO$_2$ cycle, Nature, 529, 383–386, 2016.

Pilcher, D. J., Brody, S. R., Johnson, L., and Bronselaer, B.: Assessing the abilities of CMIP5 models to represent the seasonal cycle of surface ocean pCO$_2$, J. Geophys. Res. Oceans, 120, 4625–4637, 2015.

Sabine, C. L., Feely, R. A., Gruber, N., Key, R. M., Lee, K., Bullister, J. L., Wanninkhof, R., Wong, C., Wallace, D. W. R., Tilbrook, B., Millero, F. J., Peng, T. H., Kozyr, A., Ono, T., and Rios, A. F.: The oceanic sink for anthropogenic CO$_2$, Science, 305, 367–371, 2004.

Sarmiento, J. L. and Gruber, N.: Ocean Biogeochemical Dynamics, Princeton University Press, Princeton, New Jersey, USA, 2006.

Sasse, T. P., McNeil, B. I., Matear, R. J., and Lenton, A.: Quantifying the influence of CO$_2$ seasonality on future aragonite undersaturation onset, Biogeosciences, 12, 6017–6031, https://doi.org/10.5194/bg-12-6017-2015, 2015.

Shaw, E. C., McNeil, B. I., Tilbrook, B., Matear, R., and Bates, M. L.: Anthropogenic changes to seawater buffer capacity combined with natural reef metabolism induce extreme future coral reef CO$_2$ conditions, Glob. Change Biol., 19, 1632–1641, 2013.

Steinacher, M., Joos, F., Frölicher, T. L., Bopp, L., Cadule, P., Cocco, V., Doney, S. C., Gehlen, M., Lindsay, K., Moore, J. K., Schneider, B., and Segschneider, J.: Projected 21st century decrease in marine productivity: a multi-model analysis, Biogeosciences, 7, 979–1005, https://doi.org/10.5194/bg-7-979-2010, 2010.

Takahashi, T., Olafsson, J., Goddard, J. G., Chipman, D. W., and Sutherland, S. C.: Seasonal variation of CO$_2$ and nutrients in the high-latitude surface oceans: A comparative study, Global Biogeochem. Cy., 7, 843–878, 1993.

Takahashi, T., Sutherland, S. C., Sweeney, C., Poisson, A., Metzl, N., Tilbrook, B., Bates, N., Wanninkhof, R., Feely, R. A., Sabine, C. L., Olafsson, J., and Nojiri, Y.: Global sea-air CO$_2$ flux based on climatological surface ocean pCO$_2$, and seasonal biological and temperature effects, Deep-Sea Res. Pt. II, 49, 1601–1623, 2002.

Takahashi, T., Sutherland, S. C., Chipman, D. W., Goddard, J. G., Cheng, H., Newberger, T., Sweeney, C., and Munro, D. R.: Climatological distributions of pH, pCO$_2$, total CO$_2$, alkalinity, and CaCO$_3$ saturation in the global surface ocean, and temporal changes at selected locations, Mar. Chem., 164, 95–125, 2014a.

Takahashi, T., Sutherland, S. C., Chipman, D. W., Goddard, J. G., Newberger, T., and Sweeney, C.: Climatological Distributions of pH, pCO$_2$, Total CO$_2$, Alkalinity, and CaCO$_3$ Saturation in the Global Surface Ocean, ORNL/CDIAC-160, NDP-094, Carbon Dioxide Information Analysis Center, https://doi.org/10.3334/CDIAC/OTG.NDP094, 2014b.

Taylor, K. E., Stouffer, R. J., and Meehl, G. A.: An Overview of CMIP5 and the experiment design, B. Am. Meteorol. Soc., 93, 485–498, https://doi.org/10.1175/BAMS-D-11-00094.1, 2012.

Tjiputra, J. F., Olsen, A. R. E., Bopp, L., Lenton, A., Pfeil, B., Roy, T., Segschneider, J., Totterdell, I. A. N., and Heinze, C.: Long-term surface pCO$_2$ trends from observations and models, Tellus B, 66, 23083, https://doi.org/10.3402/tellusb.v66.23083, 2014.

Valsala, V. K., Roxy, M. K., Ashok, K., and Murtugudde, R.: Spatiotemporal characteristics of seasonal to multidecadal variability of pCO$_2$ and air-sea CO$_2$ fluxes in the equatorial Pacific Ocean, J. Geophys. Res.-Oceans, 119, 8987–9012, 2014.

Völker, C., Wallace, D. W. R., and Wolf-Gladrow, D. A.: On the role of heat fluxes in the uptake of anthropogenic carbon in the North Atlantic, Global Biogeochem. Cy., 16, 1138, https://doi.org/10.1029/2002GB001897, 2002.

Zeebe, R. E. and Wolf-Gladrow, D.: CO$_2$ in Seawater: Equilibrium, Kinetics, Isotopes, Elsevier Science, Amsterdam, the Netherlands, and Philadelphia, PA, USA, 2001.